Monthly Notices of the ROYAL ASTRONOMICAL SOCIETY

MNRAS **534,** 1597–1608 (2024) https://doi.org/10.1093/mnras/stae2185
Advance Access publication 2024 September 23

INSPIRE: INvestigating Stellar Population In RElics – VII. The local environment of ultra-compact massive galaxies

Diana Scognamiglio [1]★, Chiara Spiniello [2,3], Mario Radovich [4], Crescenzo Tortora [3], Nicola R. Napolitano,[5] Rui Li [6], Matteo Maturi,[7] Michalina Maksymowicz-Maciata,[2] Michele Cappellari [2], Magda Arnaboldi,[8] Davide Bevacqua [9,10], Lodovico Coccato [8], Giuseppe D'Ago [3,11], Hai-Cheng Feng,[12] Anna Ferré-Mateu [13,14], Johanna Hartke [15,16], Ignacio Martín-Navarro[13,14] and Claudia Pulsoni [17]

[1]*Jet Propulsion Laboratory, California Institute of Technology, 4800, Oak Grove Drive, Pasadena, CA 91109, USA*
[2]*Sub-Department of Astrophysics, Department of Physics, University of Oxford, Denys Wilkinson Building, Keble Road, Oxford OX1 3RH, UK*
[3]*INAF – Osservatorio Astronomico di Capodimonte, Via Moiariello 16, I-80131 Naples, Italy*
[4]*INAF – Osservatorio Astronomico di Padova, Vicolo Osservatorio 5, I-35122 Padova, Italy*
[5]*Department of Physics 'E. Pancini' University of Naples Federico II, C.U. di Monte Sant'Angelo Via Cintia ed. 6, I-80126 Naples, Italy*
[6]*School of Physics, Zhengzhou University, Zhengzhou 450001, China*
[7]*Zentrum für Astronomie, Universität Heidelberg, Philosophenweg 12, D-69120 Heidelberg, Germany*
[8]*European Southern Observatory, Karl-Schwarzschild-Straße 2, D-85748 Garching, Germany*
[9]*INAF – Osservatorio Astronomico di Brera, via Brera 28, I-20121 Milano, Italy*
[10]*DiSAT, Universitá degli Studi dell'Insubria, via Valleggio 11, I-22100 Como, Italy*
[11]*Institute of Astronomy, University of Cambridge, Madingley Road, Cambridge CB3 0HA, UK*
[12]*Yunnan Observatories, Chinese Academy of Sciences, Kunming 650216, Yunnan, P. R. China*
[13]*Instituto de Astrofísica de Canarias, Vía Láctea s/n, E-38205 La Laguna, Tenerife, Spain*
[14]*Departamento de Astrofisica, Universidad de La Laguna, E-38200 La Laguna, Tenerife, Spain*
[15]*Finnish Centre for Astronomy with ESO (FINCA), University of Turku, FI-20014, Finland*
[16]*Tuorla Observatory, Department of Physics and Astronomy, University of Turku, FI-20014, Finland*
[17]*Max-Planck-Institut für Extraterrestrische Physik, Giessenbachstrasse, D-85748 Garching, Germany*

Accepted 2024 September 16. Received 2024 September 12; in original form 2024 July 22

ABSTRACT

Relic galaxies, the oldest ultra-compact massive galaxies (UCMGs), contain almost exclusively 'pristine' stars formed during an intense star formation (SF) burst at high redshift. As such, they allow us to study in detail the early mechanism of galaxy assembly in the Universe. Using the largest catalogue of spectroscopically confirmed UCMGs for which a *degree of relicness* (DoR) had been estimated, the INSPIRE catalogue, we investigate whether or not relics prefer dense environments. The objective of this study is to determine if the DoR, which measures how extreme the SF history was, and the surrounding environment are correlated. In order to achieve this goal, we employ the AMICO galaxy cluster catalogue to compute the probability for a galaxy to be a member of a cluster, and measure the local density around each UCMG using machine learning-based photometric redshifts. We find that UCMGs can reside both in clusters and in the field, but objects with very low DoR (< 0.3, i.e. a relatively extended SF history) prefer underdense environments. We additionally report a correlation between the DoR and the distance from the cluster centre: more extreme relics, when located in clusters, tend to occupy the more central regions of them. We finally outline potential evolution scenarios for UCMGs at different DoR to reconcile their presence in both clusters and field environments.

Key words: Galaxies: elliptical and lenticular, cD – Galaxies: evolution – Galaxies: formation – Galaxies: star formation – Galaxies: stellar content.

1 INTRODUCTION

In the Lambda cold dark matter (ΛCDM) formation scenario, the formation of massive early-type galaxies (ETGs) is consistent with a two-stage formation model (Oser et al. 2010; Naab et al. 2014). In the first stage (at $z > 2$), the central 'bulk' of mass is formed via an intense and very fast starburst that quickly ends leaving an ultra-compact quiescent galaxy, known as red nugget (Damjanov et al. 2009, 2015a). In a subsequent accretion phase, which is much more extended in time, mergers, and gas inflows cause a dramatic size growth but only minor mass change (Daddi et al. 2005; Trujillo et al. 2007; van Dokkum 2008). Although the accreted material is preferentially assembled on the outskirts of a red

★ E-mail: dianas@jpl.nasa.gov

nugget, it nevertheless contaminates, along the line of sight, the '*in situ*', pristine component that encodes the information about high-z baryonic processes, thus affecting its spatial and orbital distributions.

The stochastic nature of merging processes suggests that a non-negligible number of red nuggets at low-z should exist, having slipped through cosmic time without interacting with other systems, thus not changing their stellar populations. These very old, red, and ultra-compact nearby systems are called *relic galaxies* (Trujillo et al. 2009, 2014; Ferré-Mateu et al. 2017), as they still bear the memory of the early conditions in which they formed. Therefore, relics offer unprecedented insights into the high-z processes shaping galaxy formation and mass assembly with high precision, comparable to the study of nearby galaxies. Moreover, the number density of relics and its time evolution strongly depends on the physical processes shaping the size and mass evolution of galaxies, e.g. major and minor galaxy mergers and their relative importance, adiabatic expansion driven by stellar mass loss, and/or strong feedback (Quilis & Trujillo 2013; Furlong et al. 2015; Wellons et al. 2016; Flores-Freitas et al. 2022; Moura et al. 2024). Hence, finding and precisely counting relics in redshift bins is a very valuable way to constrain the physical scenarios driving the formation and size-evolution of massive ETGs.

It is widely acknowledged that the properties of a galaxy are significantly influenced by its surrounding environment. The past merger history should manifest in the size of ETGs, with high-density environments favouring rapid growth through dry merging (Nipoti et al. 2009; van Dokkum et al. 2010). However, studies have yielded mixed results regarding the correlation between ETG size and environment, both at intermediate redshifts and in the local Universe (Kaviraj et al. 2011; Cappellari 2013; Huertas-Company et al. 2013; Hou & Wang 2016). When restricting to UCMGs, without age and star formation histories (SFHs) distinction (i.e. relics and non-relics) the situation is unclear, with some works finding a higher number density in clusters than in the field (Poggianti et al. 2013; Stringer et al. 2015). However, this might be attributed to the fact that the majority of these studies have focussed on massive objects which are expected to be more common in denser environments at any size. For instance, Tortora et al. (2020) have performed a statistical analysis of the local environment of photometrically selected ultra-compact ($R_e < 1.5$ kpc) and massive ($M_\star > 8 \times 10^{10} M_\odot$) galaxies compared to normal-sized galaxies of similar stellar masses and colours. They have shown that the number density of UCMGs is higher in clusters only because the parent population they are derived from, i.e. red and massive ETGs, are more frequently found in these dense environments. This is also consistent to what is reported in Damjanov et al. (2015b). However, Tortora et al. (2020) have also found that the fraction of ultra-compact massive galaxies (UCMGs), calculated with respect to the total parent population in the field is slightly higher compared to that in clusters (see right panel of fig. 1 in Tortora et al. 2020).

Relic galaxies, i.e. the oldest UCMGs, containing almost exclusively stars formed during the first phase of the formation scenario, intuitively could be expected to be found in low-density environments with less hot gas in the intracluster medium (ICM). However, they have been observed also in clusters both in the local Universe (Ferré-Mateu et al. 2017, hereafter FM17) and up to $z \sim 0.7$ (Siudek et al. 2023). Hydrodynamical simulations have reached very similar conclusions, with relics being identified in clusters and field environments (Peralta de Arriba et al. 2016; Flores-Freitas et al. 2022; Kimmig et al. 2023; Moura et al. 2024). Moreover, both Flores-Freitas et al. (2022) and Moura et al. (2024), analysing relics in the Illustris TNG50 simulation, have concluded that at $z = 0$ they are closely connected to the environment in which their progenitors evolved. In particular, the progenitors of relics have been found to live in consistently higher density environments already at $z \geq 2$, while younger UCMGs residing in clusters were brought to them at a later cosmic time. However, Kimmig et al. (2023), analysing 36 quenched galaxies of stellar mass larger than 3×10^{10} M$_\odot$ at $z = 3.42$ from the Magneticum Pathfinder simulations, reached an opposite conclusion. They have found that these objects do not inhabit the densest nodes of the cosmic web, but rather sit in local underdensities.

From an observation point of view, FM17 have hinted for a possible correlation between the environment and structural, kinematics and stellar population parameters. Among the three local massive relics analysed, one was found in the field, one in a small group, and one in a cluster. Interestingly, the structural, dynamical, and stellar population properties (size, mass, and SFH) seem to be more extreme for the relic in the centre of a large cluster (NGC 1277), intermediate for the relic living in the outskirts of a small group of galaxies (PGC 032873), and less extreme for the one in isolation (Mrk 1216). This result is however based on only three objects. Now, leveraging the large data set built by INSPIRE (Spiniello et al. 2021a), we can extend this investigation, also pushing the redshift boundaries outside the local Universe.

Understanding whether systematic differences exist between UCMGs with different SFHs and living in different environments is fundamental to shed light on their origin and evolution. This is the primary objective of this study, which is the seventh of the INSPIRE series. In particular, we aim to determine the potential correlation between the local environment of UCMGs and the '*degree of relicness*' (DoR), qualitatively introduced in FM17 and quantified in Spiniello et al. (2024, hereafter INSPIRE DR3). We define the environment based on local galaxy density through two distinct methodologies. First, a cluster search is conducted utilizing the Adaptive Matched Identifier of Clustered Objects (AMICO; Bellagamba et al. 2018; Maturi et al. 2019). Secondly, the Galaxy morphoto-Z with neural Networks (GAZNETS; Li et al. 2022) is employed for precise determination of photometric redshifts and galaxy identification. Subsequent analysis explores the correlation between the environment and the DoR.

The paper is organized as follows. In Section 2, we begin by presenting the data used, starting with a brief summary of the INSPIRE Survey and its data set, followed by a description of the two catalogues employed to identify clusters, the AMICO galaxy cluster sample and the GAZNETS catalogue. In Section 3, the main analysis to measure the density of the local environment for the UMCGs is outlined. Section 4 presents our main findings, delving into the characterization of the local environment and its correlation with the DoR. We discuss the results in Section 5, also trying to relate them to possible formation scenarios. Finally, Section 6 provides a summary and conclusion for the paper.

2 DATA

Thanks to data collected as part of the ESO Large Observational programme (ID: 1104.B-0370, October 2019 to March 2023, PI: C. Spiniello), the INSPIRE project (Spiniello et al. 2021a) has built the first catalogue of spectroscopically confirmed relics outside the local Universe ($0.1 < z < 0.5$), characterizing their kinematics (D'Ago et al. 2023), stellar populations (Spiniello et al. 2021b, 2024), and low-mass end of the initial mass function (IMF; Martín-Navarro et al. 2023; Maksymowicz-Maciata et al. 2024, hereafter MM24).

Here, we use the final INSPIRE catalogue, presented in INSPIRE DR3. It comprises 52 UCMGs that were originally identified from the Kilo Degree Survey (KiDS; Kuijken 2011) DR3 footprint

(de Jong et al. 2017) via a dedicated campaign (Tortora et al. 2016, 2018; Scognamiglio et al. 2020). Among these, 38 have been confirmed as relics, as they have formed more than 75 per cent of their stellar mass during the first phase of the formation scenario (at $z > 2$). Moreover, as introduced earlier, for each of the 52 UCMGs a DoR has been computed. This is a dimensionless parameter, ranging from 0 to 1 and defined as

$$\mathrm{DoR} = \left[f_{M^{\star}_{\mathrm{tBB}=3}} + \frac{0.5\mathrm{Gyr}}{t_{75}} + \frac{0.7\mathrm{Gyr} + (t_{\mathrm{Uni}} - t_{\mathrm{fin}})}{t_{\mathrm{Uni}}} \right] \times \frac{1}{3}, \quad (1)$$

where $f_{M^{\star}_{\mathrm{tBB}=3}}$ is the fraction of stellar mass formed by $z = 2$, t_{75} is the cosmic time at which a galaxy has assembled 75 per cent of its mass, t_{fin} is the final assembly time, when 100 per cent of the stellar mass is in place. Finally, t_{Uni} is the age of the Universe at the redshift of the object. Essentially, a higher DoR indicates an earlier and more rapid mass assembly, with the most extreme relics, that have formed the entire totality of their stellar masses at $z > 2$, approaching a value of 1.[1] Conversely, UCMGs with a DoR of 0 have likely undergone a very prolonged star formation (SF), and have just stopped forming stars.

The INSPIRE UCMGs span a wide range of DoR, from 0.06 to 0.83, although having very similar sizes, $0.5 \leq R_{\mathrm{e}} \leq 1.7$ kpc, stellar masses, $0.64 \times 10^{11} \leq M_{\star} \leq 2.71 \times 10^{11}\,\mathrm{M}_{\odot}$, and colours, $1.8 \leq (g - i) \leq 2.3$. The DoR has allowed to split the 52 INSPIRE UCMGs in three main families: extreme relics (DoR > 0.7), these that have formed the totality of their stellar mass by $z = 2$, relics ($0.34 \leq$ DoR ≤ 0.7) which had formed at least 75 per cent of their stellar mass by $z = 2$, and non-relics (DoR < 0.34) characterized by a more extended SFH.

From a stellar populations point of view, by definition, the DoR correlates with the integrated stellar age. A strong correlation is also found with stellar metallicities and a mild one with the [Mg/Fe]: objects with a higher DoR have overall larger [M/H] and slightly larger [Mg/Fe] (see INSPIRE DR3). Moreover, it appears that the low-mass end of the IMF slope also correlates with the epoch of the SF (Martín-Navarro et al. 2023; MM24). Finally, relics have systematically larger velocity dispersion values than non-relics of similar stellar mass, both normal-sized and ultra-compact (MM24, INSPIRE DR3).

2.1 The AMICO galaxy cluster catalogue

The AMICO (Bellagamba et al. 2018, 2019; Maturi et al. 2019) is an algorithm for the detection of galaxy clusters in photometric surveys, based on the optimal filtering technique. It allows to maximize the signal-to-noise ratio (SNR) of the clusters (Maturi et al. 2005) taking into account the luminosity, spatial distribution, and photometric redshifts of galaxies. Briefly, AMICO searches for cluster candidates by convolving the 3D galaxy distribution with a redshift-dependent filter, which is defined as the ratio of a cluster signal, modelled with an analytical recipe, and a noise model derived directly from the data. Bayesian photo-z (BPZ; Benítez 2000), estimated from a template-fitting method, are used here. AMICO thus creates a 3D amplitude map where the candidate clusters are identified as peaks through an iterative approach designed to minimize the blending between nearby objects. The angular positions, redshift, signal amplitude, measuring the cluster galaxy abundance, and the SNR are retrieved for each cluster candidate. The mass of the cluster, based on weak lensing (WL) scaling relations, is derived too. Finally, the algorithm provides a probabilistic membership association of galaxies to clusters by exploiting the probability redshift distribution of each galaxy (provided by BPZ redshifts) and the model used for the cluster detection. The cluster model is described by a luminosity function and a radial density profile (Bellagamba et al. 2018), and observationally derived from the galaxy population of clusters detected through the Sunyaev–Zeldovich (SZ) effect (Hennig et al. 2017).

The AMICO catalogue based on KiDS DR3 data (de Jong et al. 2017) was presented in Maturi et al. (2019): it covers an area of 414 deg^2, and comprises 7988 candidate galaxy clusters at $0.1 < z < 0.8$. It has been successfully used both to derive the population properties of galaxies in the identified clusters (Radovich et al. 2020; Puddu et al. 2021), as well as for WL (Bellagamba et al. 2019; Ingoglia et al. 2022), and cosmological analyses (Giocoli et al. 2021; Lesci et al. 2022a, b; Romanello et al. 2023).

Here, we use the newest catalogue derived, applying the same algorithm on the KiDS DR4 (Kuijken et al. 2019). This catalogue, detailed in Maturi et al. (in preparation), spans a total area of 1006 deg^2, which, after masking, translates to an effective area of 840 deg^2. It includes 22 614 candidate galaxy clusters within the photometric redshift range of $0.1 < z < 0.8$, detected down to a SNR > 3.5. The catalogue has an average purity of approximately 80 per cent across the entire redshift range. However, it is worth noting that purity strongly depends on the detection SNR. We refer the readers to Maturi et al. (in preparation) for a more quantitative description of the catalogue.

2.2 The GAZNETS catalogue

The GAZNETS, introduced in Li et al. (2022), is a deep learning (DL) tool that combines both images and multiband photometry measurements for the accurate determination of photometric redshifts. What makes this tool distinctive is its integration of conventional machine learning (ML) regression tools with DL techniques. GAZNETS has been already successfully applied to a sample of galaxies from the KiDS DR4 (Kuijken et al. 2019), and tested against other ML based catalogues and classification algorithms (Khramtsov et al. 2019).

In this work, we use as input the reference network developed by Li et al. (2022), GAZNET-1, which makes use of a combination of KiDS r-band images and the KiDS + VIKING nine-bands catalogue ($ugriZYJHKs$; Wright et al. 2019). Of the 65.9 million sources in the original catalogue, roughly 40 million have a measurement in all the bands, a high-precision photometric redshift (z_{phot}), with uncertainty $\Delta z = 0.038(1 + z)$, and a corresponding probability of being classified as quasar, galaxy, or star. We use here the results obtained in Feng et al. (2024), who classified ~ 27.3 million sources with r-band magnitude ≤ 23 from the KiDS DR5 data base in quasars, galaxies, or stars using a multimodal neural network. In particular, from the classification catalogue, we pre-select only ~ 7.9 million objects that have a very high probability to being a galaxy, $P_{\mathrm{gal}} \geq 0.9$, in the redshift range $0.1 < z < 0.5$. This threshold for the P_{gal} maximizes the completeness while minimizing the contamination. Indeed, using $\sim 20\,000$ galaxies with a spectroscopic match, Li et al. (2022) have shown that, for both $P_{\mathrm{gal}} \geq 0.5$ and $P_{\mathrm{gal}} \geq 0.9$ probabilities, 99 per cent of the galaxies are classified correctly. Instead, increasing P_{gal} to 0.99, only the 78 per cent of the galaxies will be classified as such. Moreover, considering $P_{\mathrm{gal}} \geq 0.5$, 4.6 per cent of the quasi-stellar objects (QSOs) are classified as galaxies. Indeed, using $P_{\mathrm{gal}} \geq 0.5$ we would retrieve ~ 8.5 million

[1] Using the definition above, NGC 1277, the most extreme relics fully characterized in the local Universe and residing in a cluster, has a DoR ~ 0.95.

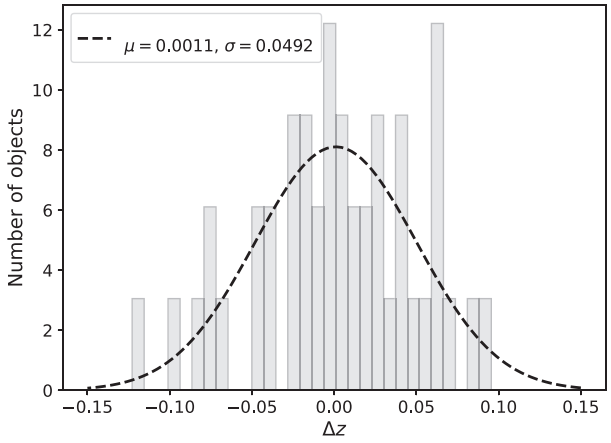

Figure 1. Distribution of the redshift difference between each INSPIRE UCMGs and the AMICO clusters at which they might be associated. The central value (μ) and standard deviation (σ) of the Gaussian distribution fitted to the histogram are shown in the legend.

of galaxies, hence hinting at a larger contamination. We nevertheless caution the reader that because the spectroscopic sample is brighter, it is easier to distinguish between quasars, galaxies, and stars.

3 ANALYSIS

In this section, we conduct an in-depth analysis of the local environment for the INSPIRE UCMGs from two perspectives. First, we investigate their potential association with galaxy cluster candidates by cross-referencing INSPIRE catalogue data with the AMICO catalogue. We focus on evaluating the probability of UCMGs being members of these clusters and its possible correlation with the DoR. Secondly, we measure the local density around each INSPIRE UCMG by conducting a cross-match with the GAZNETS catalogue and counting galaxies with compatible redshifts. Through this analysis, we aim to determine whether a statistically significant overdensity exists, thereby indicating a cluster environment, and its correlation with the DoR.

3.1 Cluster membership from AMICO

For each cluster candidate, AMICO provides a list of galaxies with the probability of being a cluster member ($P_{\rm cluster}$). The $P_{\rm cluster}$ is computed through a cluster model, which assumes a luminosity function and a radial density profile. We note that the probability is distance-dependent in the sense that galaxies spatially more distant from the cluster centre will, by construction, have a lower probability. We cross-match the list of galaxies that could be a member of one of the AMICO clusters with the 52 INSPIRE UCMGs, finding that 45 out of the 52 INSPIRE UCMGs have $P_{\rm cluster} > 0$. However, only nine of them have a probability of being members greater than or equal to 0.5 (i.e. $P_{\rm cluster} \geq 0.5$), which means that their probability to be in a cluster is larger than their probability to be in the field. We will denote these as 'safe' detections for the remainder of this paper.

In Fig. 1, we show the distribution of the redshift difference, $\Delta z = (z_{\rm UCMG} - z_{\rm cluster})/(1 + z_{\rm UCMG})$, between each of the 45 UCMGs with a match and the corresponding AMICO cluster. The redshifts exhibit close proximity, with a mean $\Delta z = 0.0011$ and a standard deviation $\sigma = 0.0492$, as reported in the legend, although there is one object with $|\Delta z| > 0.1$ (J0844+0148, $z_{\rm UCMG} = 0.2837$, $z_{\rm cluster} = 0.4413$). We stress that the clusters' redshifts are based on the photometric redshifts of their members.

The results of the cross-matching between the AMICO cluster catalogue and INSPIRE galaxies are listed in the second block of columns of Table 1, where we list, for the 45 objects with a match, the redshift of the AMICO cluster compatible with that of the UCMG, the probability of the object to be a member of that cluster, the SNR of the detection, the level of the purity ($\mathscr{P}$), and the virial mass of the cluster (M_{200}). The seven objects that lack a match in AMICO are still listed in the table but without a numerical value for these quantities. In fact, for these, the cluster-finding algorithm does not find a suitable association to any of the detected cluster candidates. This suggests that they might be field galaxies or reside in groups of galaxies that are too small to be detected by AMICO.

The 45 INSPIRE galaxies matched with the AMICO cluster candidates exhibit a broad range in DoR, as visible from Fig. 2, where we colour-coded the data points by the purity of the cluster, $\mathscr{P}$. In the same figure, the remaining seven UCMGs without a match are illustrated as black crosses at $P_{\rm cluster} = 0$. A linear relation, showed as a grey dashed line, emerges when we restrict to 'safe' detections, i.e. limiting to points with $P_{\rm cluster} \geq 0.5$, corresponding to a 50 per cent probability of belonging to the cluster identified by the algorithm.

In summary, according to the analysis carried out from AMICO, nine objects are members of a cluster of galaxies ($P_{\rm cluster} \geq 0.5$), while seven are most likely in the field with a high degree of confidence as they do not have a match. The remaining 36 objects exhibit a wide range of $P_{\rm cluster}$ values, but all lower than 0.5, hence preventing a safe classification of the local environment. Considering the grouping from INSPIRE DR3, all nine extreme relics (DoR > 0.7) have a match with an AMICO cluster. Of the seven UCMGs lacking a match in AMICO, six are relics ($0.34 \leq$ DoR < 0.7) and one is a non-relic (DoR< 0.34). There are two extreme relics, four relics, and three non-relics with $P_{\rm cluster} \geq 0.5$. Henceforth, there appears to be no clear environmental preference for UCMGs with varying degree of relicness but that a linear correlation exists between DoR and $P_{\rm cluster}$ for the 'safe' detections ($P_{\rm cluster} \geq 0.5$). Furthermore, we notice that UCMGs with a very extended SFH (DoR < 0.3) all show rather low probabilities of being in a cluster.

3.2 Overdensities identification from the GAZNETS catalogue

In this section, we describe the cross-match between the INSPIRE catalogue and the GAZNETS galaxy catalogue described in Section 2.2. We select, for each of the 52 UCMGs, all and only galaxies (objects with $P_{\rm gal} \geq 0.9$ in the catalogue by Feng et al., submitted) having redshift compatible to that of the INSPIRE objects and $m_r < 22$. In particular, for the redshift, we compute $\Delta z = (z_{\rm UCMG} - z_{\rm phot})/(1 + z_{\rm UCMG})$ and retrieve objects with $|\Delta z| \leq 0.03$. To justify our choices in magnitude and redshift range, we use spectroscopic data from the Dark Energy Spectroscopic Instrument (DESI) Survey (Levi et al. 2019; DESI Collaboration 2023). We cross-match the catalogue with the GAZNETS one and check the precision of the ML photometric redshifts against the spectroscopic ones. For objects brighter than $m_r < 22$, the uncertainty in redshift estimation is of the order of 0.03, while it increases for fainter objects. Furthermore, we also point the reader to fig. 3 in Li et al. (2022), where the accuracy of the GAZNETS ML photometric redshifts is estimated on the training sample of 20 000 galaxies used to test the performances of the ML models. We restrict our analysis to galaxies with $m_r < 22$, corresponding to detecting galaxies with $M_\star + 5$ at $z = 0.1$ and $M_\star + 2$ at $z = 0.4$ for the redshifts of the UCMGs. For each galaxy in INSPIRE meeting this criterion and having $|\Delta z| \leq 0.03$, we

Table 1. Classification of the local environment for the 52 INSPIRE UCMGs. 9 objects are in an overdense region (top rows) with high degree of confidence, 17 definitively in underdense environments (middle rows). For the remaining, only a tentative environment classification is provided. Within each environment group (horizontal lines), galaxies are ordered in descending order of DoR. We list the INSPIRE ID, the DoR and, the redshifts of the UCMGs ($z_{\rm UCMG}$) in the first vertical block (from INSPIRE DR3). In the second block, we list quantities derived from AMICO: redshift of the cluster ($z_{\rm cluster}$), the probability for the UCMG to belonging to that cluster ($P_{\rm cluster}$), the signal-to-noise ratio (SNR) of detection, its purity ($\mathscr{P}$), the cluster's virial mass in $M_\odot$ ($M^{200}_{\rm cluster}$), and the logarithmic distance of the UCMG from the cluster centre in kpc ($\log D_{\rm A}$). Finally, in the third block, we list the overdensity value (δ_Σ), the logarithmic distance of each UCMG from its centre in kpc ($\log D_{\rm GZ}$), both derived from GAZNETS, and lastly, the environment classification. Rows corresponding to objects without a match in AMICO or GAZNETS are listed with a –.

ID INSPIRE	DoR	$z_{\rm UCMG}$	$z_{\rm cluster}$	$P_{\rm cluster}$	SNR	$\mathscr{P}$	$M^{200}_{\rm cluster}$ ($M_\odot$)	$\log D_{\rm A}$ (kpc)	δ_Σ	$\log D_{\rm GZ}$ (kpc)	Environment
J0211−3155	0.72	0.3012	0.2714	0.79	4.84	0.88	13.505	2.52	5.36	2.78	C
J2359−3320	0.71	0.2888	0.2913	0.91	7.87	1.00	14.149	2.51	12.98	2.48	C
J0920+ 0212	0.64	0.2800	0.2913	0.80	5.85	0.98	13.871	2.66	11.59	2.86	C
J0314−3215	0.42	0.2874	0.2616	0.65	6.09	0.99	14.125	2.85	12.04	2.90	C
J0844+0148	0.45	0.2837	0.4413	0.61	3.96	0.53	13.528	2.44	4.64	3.10	C
J1202+0251	0.36	0.3298	0.3216	0.58	4.28	0.72	13.428	2.73	7.04	2.76	C
J1436+0007	0.33	0.2210	0.2517	0.77	6.30	1.00	13.647	2.58	3.32	3.16	C
J0904−0018	0.32	0.2989	0.3216	0.56	4.69	0.88	13.719	2.83	5.81	2.63	C
J1402+0117	0.31	0.2538	0.2616	0.62	7.31	1.00	14.089	3.05	17.06	3.00	C
J1438−0127	0.78	0.2861	0.3013	0.10	4.48	0.88	13.266	3.40	2.51	3.06^{+}	F
J1412−0020	0.61	0.2783	–	–	–	–	–	–	2.10	2.71^{+}	F
J1457−0140	0.47	0.3371	0.2419	0.12	3.47	0.27	13.027	3.33	2.86	3.10^{+}	F
J2356−3332	0.44	0.3389	0.2813	0.10	3.12	0.53	12.701	3.29	0.54	3.14^{+}	F
J0918+0122	0.43	0.3731	0.4647	0.007	3.82	0.54	13.262	2.90	2.24	2.48^{+}	F
J1411+0233	0.41	0.3598	0.3427	0.17	4.06	0.62	13.724	3.21	1.51	2.46^{+}	F
J1420−0035	0.41	0.2482	0.3427	0.17	5.72	0.99	13.916	3.12	2.37	1.85^{+}	F
J1114+0039	0.40	0.3004	0.4289	0.01	4.25	0.72	13.461	3.34	2.99	3.09^{+}	F
J0316−2953	0.40	0.3596	0.4647	0.03	3.66	0.40	13.178	3.22	2.81	2.43^{+}	F
J1527−0012	0.38	0.4000	–	–	–	–	–	–	2.35	2.32^{+}	F
J1527−0023	0.37	0.3499	–	–	–	–	–	–	2.81	3.14^{+}	F
J0321−3213	0.37	0.2947	0.3537	0.03	3.70	0.47	13.516	3.47	1.45	2.48^{+}	F
J2257−3306	0.27	0.2575	0.2913	0.15	4.26	0.72	13.108	3.27	2.72	3.05^{+}	F
J0920+0126	0.25	0.3117	–	–	–	–	–	–	2.29	3.09^{+}	F
J1142+0012	0.18	0.1077	0.0951	0.28	2.88	0.00	12.744	3.06	2.43	3.10^{+}	F
J0226−3158	0.12	0.2355	0.2913	0.19	3.04	0.14	12.981	3.03	2.56	2.93^{+}	F
J2327−3312	0.06	0.4065	0.2913	0.27	4.21	0.70	13.293	3.28	2.34	2.40^{+}	F
J2305−3436	0.80	0.2978	0.2616	0.007	3.38	0.53	13.077	3.47	6.06	2.26	C*
J2204−3112	0.78	0.2581	0.3652	0.07	4.59	0.76	13.255	3.27	5.53	2.89	C*
J1040+0056	0.77	0.2716	0.2223	0.25	6.48	1.00	13.736	2.74	8.14	2.81	C*
J1449−0138	0.60	0.2655	0.3114	0.23	4.81	0.88	13.595	3.17	6.57	3.14	C*
J0838+0052	0.54	0.2702	0.1929	0.36	3.83	0.47	13.549	2.80	6.19	2.56	C*
J0240−3141	0.43	0.2789	0.2714	0.25	4.62	0.76	13.598	3.22	9.61	3.17	C*
J1228−0153	0.39	0.2973	0.1733	0.07	3.49	0.53	13.042	3.32	10.54	3.17	C*
J1447−0149	0.38	0.2074	0.2321	0.42	5.69	0.99	13.438	3.11	10.77	3.17	C*
J2312−3438	0.36	0.3665	0.3652	0.25	3.31	0.31	13.172	2.64	9.45	2.78	C*
J1414+0004	0.36	0.3030	0.2223	0.36	3.92	0.53	13.113	3.00	5.33	3.18	C*
J1154−0016	0.11	0.3356	0.2517	0.18	6.44	0.53	13.899	3.53	5.44	3.17	C*
J0847+0112	0.83	0.1764	0.2027	0.14	3.36	0.26	12.963	3.24	3.68	2.32	F*
J0909+0147	0.79	0.2151	0.1538	0.01	2.89	0.00	12.853	2.91	4.19	3.17	F*
J0842+0059	0.73	0.2959	0.3216	0.09	3.35	0.27	13.035	3.34	3.48	2.46	F*
J0224−3143	0.56	0.3839	0.3114	0.15	4.88	1.00	13.445	3.43	3.38	3.16	F*
J0317−2957	0.51	0.2611	–	–	–	–	–	–	3.87	2.45	F*
J2202−3101	0.48	0.3185	–	–	–	–	–	–	4.38	2.91	F*
J1218+0232	0.45	0.3080	–	–	–	–	–	–	4.64	3.18	F*
J0917−0123	0.44	0.3602	0.3013	0.19	3.45	0.31	12.292	3.11	4.07	2.18	F*
J0857−0108	0.39	0.2694	0.1929	0.18	3.43	0.27	13.163	2.92	4.56	2.40	F*
J1128−0153	0.34	0.2217	0.1831	0.24	5.13	0.97	12.798	3.34	3.54	3.17	F*
J1417+0106	0.33	0.1794	0.1831	0.27	3.78	0.54	12.610	3.08	3.50	3.03	F*
J1156−0023	0.30	0.2552	0.2616	0.27	9.02	1.00	14.421	3.40	3.22	3.16	F*
J0326−3303	0.25	0.2970	0.2714	0.11	4.06	0.34	13.105	3.39	3.60	2.91	F*
J1026+0033	0.29	0.1743	0.1440	0.09	2.91	0.14	12.918	3.28	–	–	F*
J1456+0020	0.17	0.2738	0.3216	0.09	3.85	0.47	13.409	3.29	3.15	2.25	F*

Notes. $^{+}$The distances have been calculated from the nearest density peak, which is, however, not significant compared to the background level *Tentative environment classification (see the text for more details).

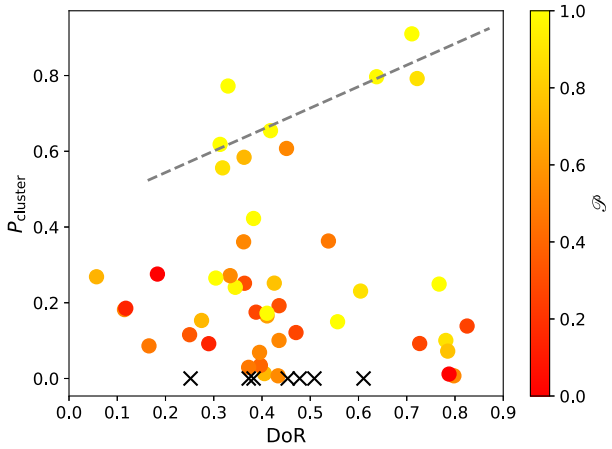

Figure 2. Probability to belong to a cluster according to AMICO against the DoR for the 45 INSPIRE UCMGs with a match in AMICO, colour-coded by the purity. The seven objects without a match are visualized as crosses at $P_{\rm cluster} = 0$. When restricting to 'safe' detections (galaxies with $P_{\rm cluster} \geq 0.5$, see the text for more details), a linear relation (dashed line) is found, with higher probabilities for objects with larger DoR.

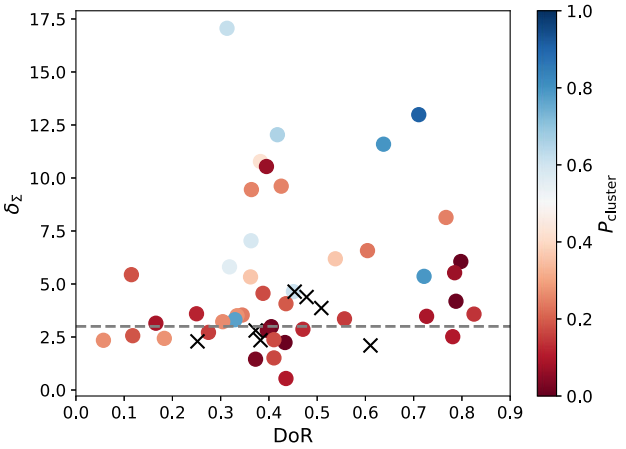

Figure 3. Overdensity as a function of the DoR for the 51 INSPIRE UCMG for which a $\delta_{\Sigma,\rm min}$ could be computed. The dashed line represents the threshold $\delta_{\Sigma,\rm min}$ for an overdensity to be significant. The data points are colour-coded by their probability to reside in an AMICO cluster and the seven objects without a match in AMICO are visualized as crosses.

generate a density map within a 10 Mpc radius. This is accomplished using KDEPY[2] library that performs a kernel density estimation (KDE) on both 1D and 2D data. Specifically, we employ an Epanechnikov kernel (Epanechnikov 1969) with a bandwidth of 0.2 Mpc. We extract the peak of the density within a radius of 1.5 Mpc ($\sim r_{200}$ for a cluster with $M^{200}_{\rm cluster} \sim 10^{14} - 10^{14.5}{\rm M}_\odot$), to check for the presence of nearby overdensities (next nearest neighbour, $\Sigma_{\rm NNB}$). We then select 50 random regions all located from 5 to 9 Mpc from the UCMG and all with radius of 1.5 Mpc. We compute the mean and standard deviation of this distribution ($\Sigma_{\rm BKG} \pm \sigma_{\Sigma_{\rm BKG}}$), using it as a background estimation. Practically speaking, with this procedure, we are estimating the significance of an overdensity in the proximity of each UCMG by the quantity

$$\delta_\Sigma = \frac{\Sigma_{\rm NNB} - \Sigma_{\rm BKG}}{\sigma_{\Sigma_{\rm BKG}}}. \quad (2)$$

To determine the threshold in δ_Σ for which we expect that an overdensity is significant, we repeat the procedure, while randomizing the galaxy positions in the field. The threshold is then defined as the average value of δ_Σ calculated in these randomized fields, which is $\delta_{\Sigma,\rm min} = 3$. For one galaxy, J1026+0033, it has not been possible to compute the value of $\delta_{\Sigma,\rm min}$. This object lies in proximity to a luminous star, which has been masked in the catalogues, causing a non-homogeneous mapping of the proximity of the UCMGs.

Fig. 3 shows the overdensity (δ_Σ) values measured for each UCMG against their DoR. The dashed grey lines represent the δ_Σ threshold for an overdensity to be significant. The data points are colour-coded by the $P_{\rm cluster}$ and those without a match in AMICO are visualized as black crosses.

We observe a similar behaviour to that described in the previous section (Section 2.1, Fig. 2). Nearly all UCMGs with extended SFHs (DoR < 0.3) prefer underdense environments. However, the scatter suddenly intensifies at intermediate DoR, where UCMGs reach values of δ_Σ as high as 17.06 and as low as 0.54. The data points in the figure are colour-coded by the probability to reside in an AMICO cluster. All objects with $P_{\rm cluster} \geq 0.5$, i.e. 'safe' detection, pass the δ_Σ threshold (grey dashed line). This result serves as a confirmation of the consistency between the two methods.

Interestingly, the vast majority of galaxies with DoR ≥ 0.5 are positioned above the δ_Σ, suggesting, once again, that relics might slightly prefer overdense environments, such as clusters of galaxies. Specifically, almost all (eight out of nine) extreme relics and two-thirds of relics with intermediate DoR values are above the threshold (with the maximum scatter), while roughly 50 per cent of the non-relics fall below the significance threshold. Only 1 out of the 14 non-relics has a very high value of δ_Σ (J1402+0117, $\delta_\Sigma = 17.06$[3]).

Hence, according toGAZNETS, 34 INSPIRE UCMGs (65 per cent of the sample) reside in overdensities ($\delta_\Sigma \geq 3$). Of these, 8 (out of 9) are extreme relics, 8 are non-relics (out of 14), and only 3 (out of 9) have DoR < 0.3.

4 RESULTS: CHARACTERIZATION OF THE LOCAL ENVIRONMENT

In this section, we present the results of the analysis performed in the paper, focussing on the relation between the DoR and the environments occupied by the UCMGs. This topic was already introduced in previous papers (e.g. Poggianti et al. 2013; Stringer et al. 2015; Damjanov et al. 2015b; Tortora et al. 2020), which, however, lack any distinction between the ancient massive relics of the early Universe from relatively younger but equally compact and massive systems, that have undergone a much more extended SF. In the local Universe, FM17, based on three confirmed relics, hinted for a correlation between the kinematics, structural, and stellar population parameters of three extreme relics and their local environment. The great step forward brought by INSPIRE is the possibility to investigate on this matter with a much larger number statistics and covering a wider range in DoR. Hence, we have checked whether an environmental dependency exists for the stellar masses and sizes (Scognamiglio et al. 2020), velocity dispersion values (D'Ago et al. 2023), and stellar parameters (IMF slope, metallicity, [Mg/Fe]; MM24). Surprisingly, no statistically significant correlation

[2]https://kdepy.readthedocs.io

[3]From the map shown in Fig. 7, this galaxy seems to lie within two groups/clusters.

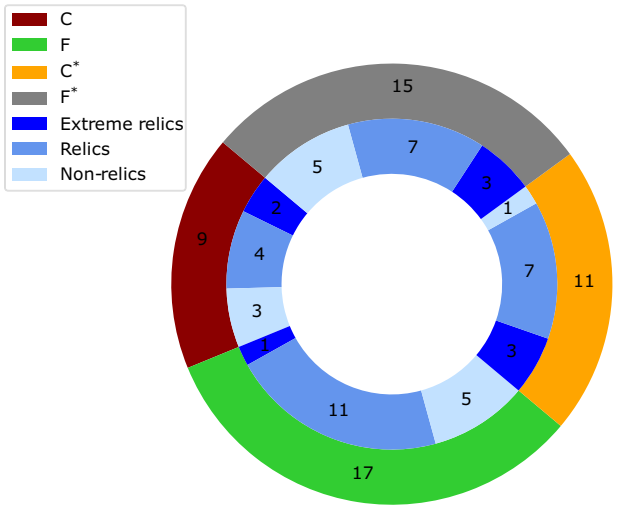

Figure 4. Summary of number of INSPIRE UCMGs for each environment (outer circles), and DoR family (inner circles).

was found, indicating that the larger INSPIRE sample does not support the idea hinted at in FM17. Velocity dispersion and stellar population parameters, although varying as a function of DoR, do not depend upon the density of the local environment in which an UCMG resides.

Table 1 provides a summary of the characterization of the local environments for the 52 INSPIRE UCMGs. The first (second) horizontal block of the table lists objects that are residing in an over(under)dense region with high degree of confidence, having very high (low) values of both $P_{\rm cluster}$ and δ_Σ. Among the 26 UCMGs whose environment can be confidently determined (50 per cent of the sample), 9 are situated in clusters (labelled as 'C') and 17 in the field (labelled as 'F'). These galaxies exhibit a diverse range of DoR values in both environments. Notably, we confirm the absence of UCMGs with DoR < 0.3 in cluster environments. Out of the remaining 26 INSPIRE objects, 11 are likely to be cluster members, while 15 might inhabit either field environments or small galaxy groups, although a definitive determination remains uncertain. Specifically, the objects marked as 'C*' in Table 1 exhibit a significant δ_Σ value, exceeding the threshold by more than 1σ, yet they have an AMICO $P_{\rm cluster}$ value below 0.5. This implies that they reside within an overdense region. Their low AMICO probability could stem from different factors, such as the UCMGs being situated relatively far from the cluster centre,[4] or due to potential inaccuracies in the photometric redshift estimation of the cluster. Lastly, systems denoted with an 'F*' have a δ_Σ slightly above the threshold (but less than 1σ away), along with a low $P_{\rm cluster}$ value, likely reside in the field or in the outskirts of a small galaxy group, with moderate density. The wedge plot in Fig. 4 provides a graphical visualization of the numbers of UCMGs based on the environment classification (outer circle) and on the three families defined in INSPIRE DR3 according to the DoR (inner circle).

Fig. 5 shows four of the most extreme INSPIRE objects (two highest and two lowest DoRs), for which a definitive estimate of the local environment could be obtained (i.e. first two blocks of Table 1). The two objects on the top row are two extreme relics with DoR > 0.7, one of them is in a cluster one in the field. The bottom

[4]We remind the reader that $P_{\rm cluster}$ is distance-dependent.

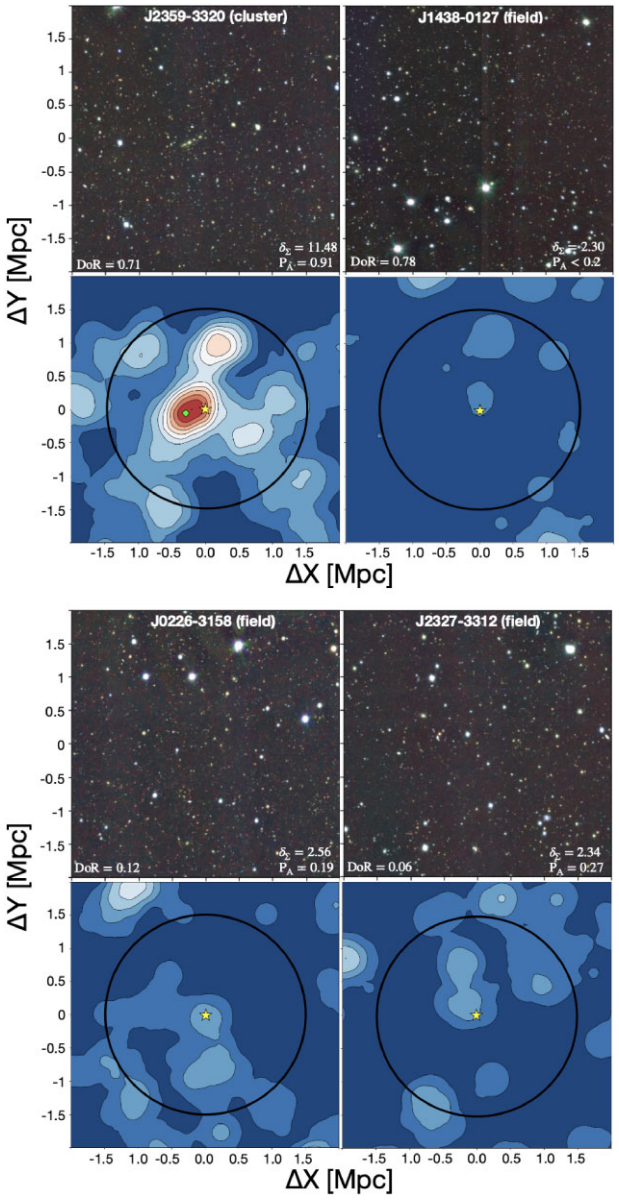

Figure 5. KiDS *gri* cut-outs (top panels) and KDE density maps (bottom panels) of size 2×2 Mpc^2 for the objects with highest (top row) and lowest (bottom row) DoR in the INSPIRE sample, for which a definitive environment characterization has been obtained. The cut-outs also display DoR, $P_{\rm A}$, and δ_Σ values. The subscript 'A' is used to denote the $P_{\rm cluster}$ from 'AMICO', for brevity and clarity in the images. In the KDE density maps, the star indicates the position of the UCMG, while the diamond identifies the cluster centre, if any. The circular aperture of 1.5 Mpc used to identify the nearest overdensity is also drawn on the map in black.

row depicts instead two objects with the lowest DoR, all in the field according to our classification. For each galaxy, the top panel illustrates the *gri* colour-combined image from the KiDS survey while the bottom shows the KDE density map, both with size of 2×2 Mpc^2 and centred on the UCMG, which is plotted as a yellow star in the maps. For objects in clusters, we also highlight the position of the centre of the cluster candidate as a green diamond. Fig. 6 shows instead four objects with very similar DoR (intermediate ~ 0.4) but residing in different environments. The two top systems live in an overdensity, while the two bottom ones inhabit underdense

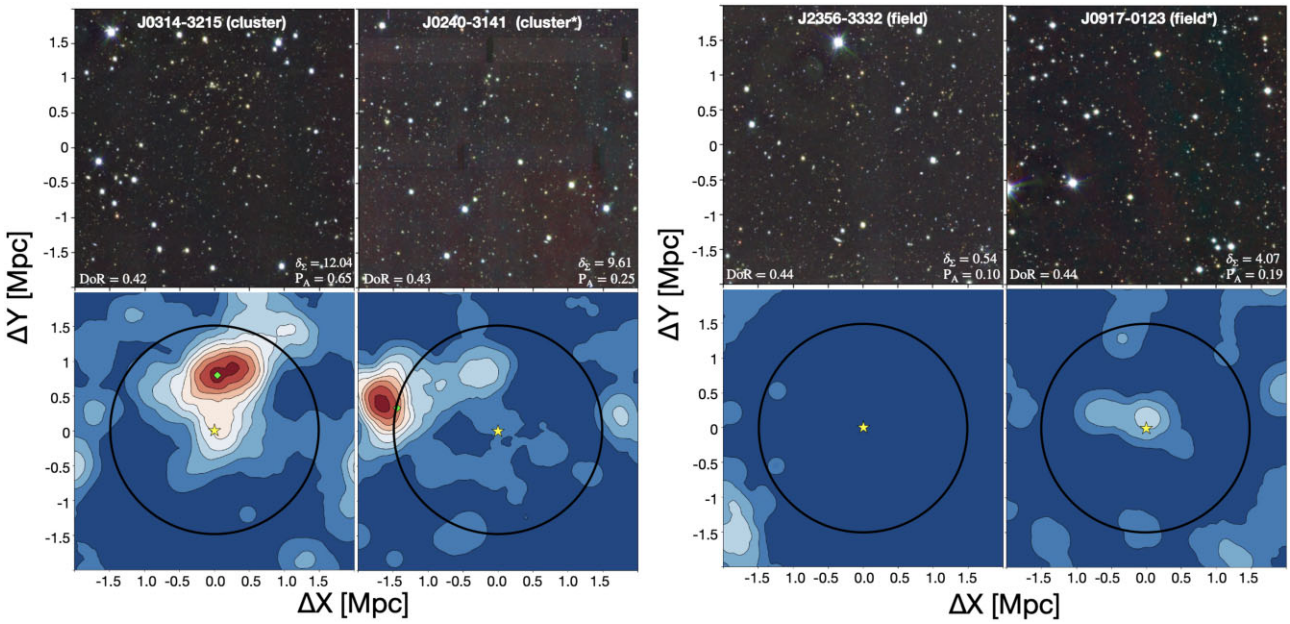

Figure 6. The same as in the previous figure, but for four INSPIRE UCMGs with intermediate DoR residing in different environments (cluster on the left, field on the right). We display two 'safe' classifications and two tentative ones. Symbols and scales are as in the previous figure.

environments. In all panels, the ID, DoR, δ_Σ, and $P_{\rm cluster}$ (reported as $P_{\rm A}$, for brevity and clarity in the images) values are reported. Finally, Fig. 7 shows the KDE maps for additional 10 objects, 5 in overdense and 5 in underdense environments to provide a general idea of the variety of the maps for the INSPIRE sample. Objects in the same column (top and bottom) have very comparable DoR values. Moving from left to right within the same row, the δ_Σ values decrease.

4.1 Correlation between the DoR and the UCMG distance to the cluster centre

In Table 1, we include the logarithmic values of the distance of an UCMG from both a cluster centre and from an overdensity, in kpc. These values are visualized in Fig. 8, where they are plotted against the DoR. In this figure, the dark red points represent AMICO data, while the blue points denote GAZNETS data. Galaxies confidently identified as belonging to a cluster or an overdensity are labelled with 'C', whereas those considered tentative members are marked with 'C*' (shaded circles). For both methods, a similar correlation is found: the higher the DoR, the closer to the cluster centre/overdensity the UCMGs is located. Indeed, performing a linear fit between the aforementioned distances and the DoR values, a comparably negative correlation is evident in both cases:

$$\log_{10} D_{\rm AMICO} = 3.02 - (0.7 \times {\rm DoR})$$
$$\log_{10} D_{\rm GaZNets} = 3.13 - (0.6 \times {\rm DoR}). \quad (3)$$

To assess the significance of the correlation between the DoR and the $\log_{10} D$ for the 'safe' detections, we perform a bootstrap analysis. We randomize the DoR and $\log_{10} D$ values independently for 49 iterations and include the original data as the 50th iteration. The mean slope from these bootstrapped data sets is $\mu = 0.01 \pm 0.46$ for AMICO and $\mu = -0.04 \pm 0.43$ for GAZNETS. In contrast, the slopes from the original data are 0.7 for AMICO and 0.6 for GAZNETS. These significant differences indicate that the observed correlations are not due to random fluctuations, affirming the robustness and significance of the relationship between DoR and $\log_{10} D$.

It is worth noting that the physical significance of the distance from the centre varies significantly depending on whether one considers a very massive cluster of galaxies, which can extend up to much larger distances or small groups, that are instead generally much smaller in size. Nevertheless, from Table 1 it is clear that the cluster candidates identified by AMICO do not exhibit a wide range in total mass, spanning from 4.1×10^{12} to $2.6 \times 10^{14}\,{\rm M}_\odot$, and with a mean and standard deviation of $(2.6 \pm 0.1) \times 10^{13}\,{\rm M}_\odot$. Finally, we also note that the distance–DoR relation shows a much larger scatter and a shallower slope when considering all the UCMGs that are tentatively residing in a cluster (i.e. C*, shaded dark red points in Fig. 8). However, as already stressed, the quantities derived by AMICO are based on the detection algorithm that depends on less-precise photometric redshifts and on the analytical cluster model based on a luminosity function and a radial density profile. Furthermore, sometimes a system could be associated (through the membership probability) to more than one cluster. Hence, the estimate of the log D for AMICO, especially for tentative classification, could be biased or influenced by unaccounted factors. The overdensity values from GAZNETS are based on more accurate ML redshifts and simply trace the number of galaxies in the proximity of each UCMG, without assuming any model or light distribution.

5 DISCUSSION

From this study it has emerged that UCMGs are present in both over and underdense regions, in line with what previously reported (Damjanov et al. 2015b; Tortora et al. 2020). We further found that there is no correlation between their DoR and the density of the local environment. Our observational findings are in perfect agreement by results from simulations (Moura et al. 2024), which have shown that both relics and younger UCMGs exhibit no distinct preference towards either high- or low-density environments at $z = 0$. Instead, they are distributed across a range of densities, as evidenced by their presence in various environments.

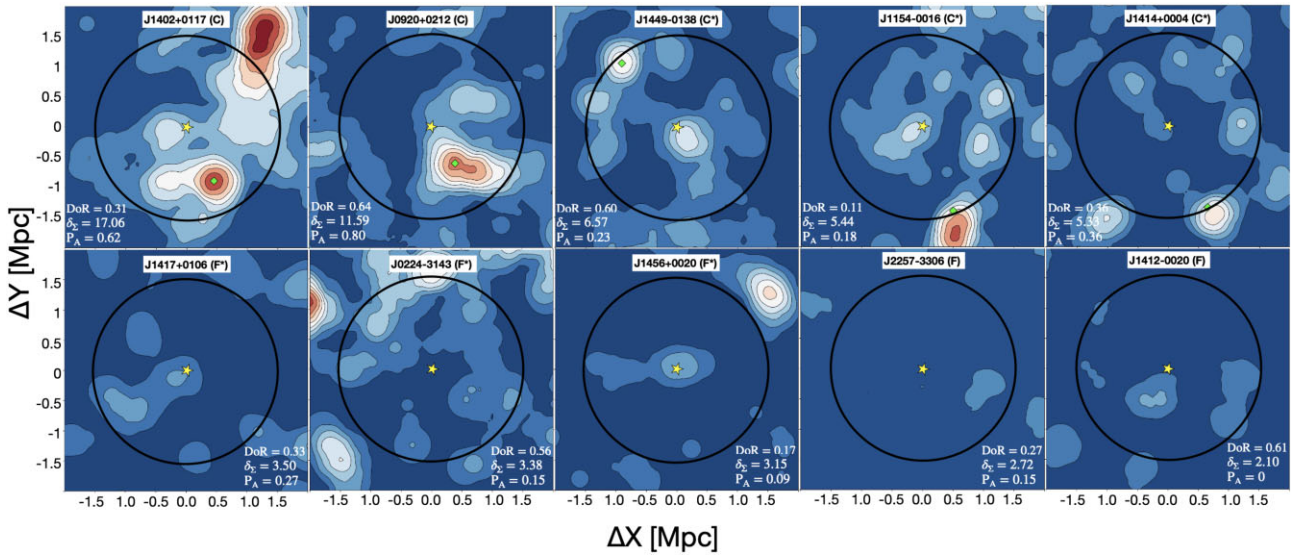

Figure 7. KDE density of 2×2 Mpc^2 for five objects in overdense environments (top row) and five objects in underdense environment (bottom row), ordered by their δ_Σ value. Symbols as in the previous figures.

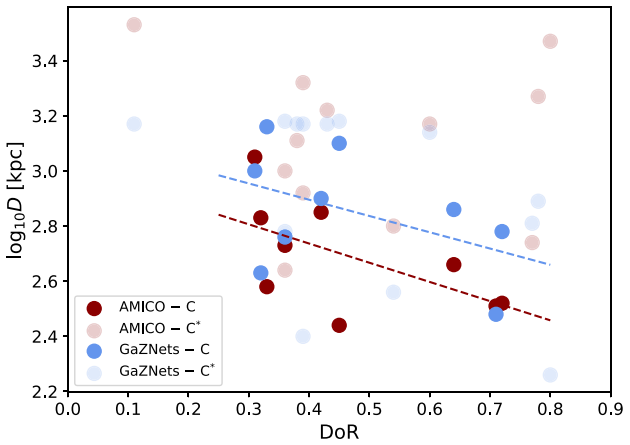

Figure 8. Correlation between DoR and distances from a cluster candidate or an overdensity, for AMICO (dark red points) and GAZNETS (blue points), labelled with 'C' in Table 1. A linear fit is shown as dashed line for both cases. Lighter points show the UCMGs labelled as 'C*' in Table 1, which are not included in the fit as the classification of the environment is tentative.

In this section, we focus on possible evolutionary scenarios that are able to explain the presence of UCMGs with all DoR both in over and underdense regions and possibly, the lack of objects with DoR< 0.3 in cluster environment. We start by focussing on the most extreme relics, hypothesizing on how they could avoid any interaction with other cluster members or very quickly stop forming stars in the field. We then focus on UCMGs with a very extended SFH, which seem to prefer underdense environments. Finally, we stress that a possible third scenario might exist for UCMGs with low and intermediate DoR. Indeed, the observed near-by UCMGs might also be galaxies that had a three phase formation and evolution scenario. After the size growth phase they might have gone through a subsequent phase of re-compaction due to stripping and gas removal (Kapferer et al. 2009; Peluso et al. 2022; Göller et al. 2023), and are therefore observed to be ultra-compact today. This is highly unlikely for extreme relics, where the entire totality of the stellar population is almost as old as the Universe but it cannot be excluded for the remaining cases.

5.1 Extreme relics in clusters and in the field

Among the nine extreme relics (DoR > 0.7) which have formed all their stellar mass at high-z, two are in an overdense environment and one is in an underdense region (J1438−0127, DoR $= 0.78$) with a high degree of confidence. For the remaining six systems, three are likely to reside in clusters or groups and three more likely to be in the field. Moreover, when extreme relics are in a cluster, they tend to be closer to its centre than UCMGs with lower DoR.

While it is quite intuitive to understand how a high-z isolated, field red nugget can evolve passively and undisturbed through cosmic time without interacting with any other system, it is difficult to explain how it can survive untouched for many Gyr in the central regions of a cluster/group of galaxies. A plausible explanation is that extreme relics have a very deep potential well and incredibly high density, which make them less susceptible to interactions with other galaxies (see also Poggianti et al. 2013). This scenario is also supported by the fact that extreme relics have a larger stellar velocity dispersion (up to ~ 400 km s^{-1} at $M_\star \sim 10^{11}$M$_\odot$) than non-relics, both younger UCMGs and normal-sized ETGs, of similar stellar mass (Ferré-Mateu et al. 2017; Spiniello et al. 2021b, 2024; Grèbol-Tomàs, Ferré-Mateu & Domínguez-Sánchez 2023). As found in Peralta de Arriba et al. (2016), the high-velocity dispersion values and the hot ICM can prevent the growth of an accreted stellar envelope through mergers. Furthermore, a dense environment could help in preventing a continuous SF. Indeed, stripping of the cold gas surrounding a galaxy might happen by the hot, dense diffuse intra-cluster gas, causing SF to cease (Ma et al. 2008; Bekki 2013; Roediger et al. 2014; Steinhauser, Schindler & Springel 2016; Foltz et al. 2018). Finally, the so-called 'galaxy harassment', which is the combined effect of gravitational interactions between galaxies (Merritt 1983; Bialas et al. 2015) and their interaction with the potential well of the cluster as a whole (Byrd & Valtonen 1990), has often been proposed to explain the formation of red-sequence galaxies (e.g. Boselli & Gavazzi 2014). So, if the UCMGs entered in the cluster very early-on in time, or formed with it, they stopped forming stars and then evolved passively thereafter.

Our findings align well with the theoretical scenario described in Moura et al. (2024). The authors have shown that, although in the

local Universe relics and younger compact galaxies can be found in all environments, at $z > 2$ the number of relics in clusters is higher when compared to younger UCMGs at the same mass range (see also Kimmig et al. 2023). Hence, red nuggets that will be progenitors of relics were preferentially in an overdensity at high-z. On the contrary, ultra-compact non-relics in a cluster entered in this dense environment only at later stages.

In low-density environments, instead, red nuggets are less likely to merge and increase the '*ex situ*' fraction of stars. Therefore, we expect to find these ultra-compact systems still as such in more isolated environment (Peralta de Arriba et al. 2016; Kimmig et al. 2023; Moura et al. 2024). However, if the red nuggets are surrounded by a gas reservoir, they might keep forming stars, although at a very low-rate until they consume it. Hence, extreme relics in the field might be the local descendants of red nuggets have been formed in gas-poor underdense regions of the Universe at early epochs. This might be the case of J1438−0127, the only INSPIRE extreme relic (DoR = 0.78) in the field, and Mrk1216, the only near-by extreme relic definitively the field.

5.2 Why do UCMGs with more extended SFHs prefer the field?

At the other extreme of the distribution, we have found no objects with DoR ≤ 0.3 definitively located in an overdense region. Looking at the tentative classifications [marked with an asterisk (∗) in Table 1], only 1 out of 10 UCMGs with such lower DoR could be in a cluster. Among the remaining objects, six are definitively in underdense regions and three are tentatively in the field. These objects, although passive and relatively old ($\sim$ 4–6 Gyr) in an integrated sense, are characterized by a much more extended SFH and they are still forming a small percentage of their stellar mass today or stopped very recently, similar to those originally found in Trujillo et al. (2009) and Ferré-Mateu et al. (2012). The preference for UCMGs with extended SFHs to live in the field could be explained by the fact that in these underdense environments, major (and especially dry) mergers are rare (e.g. de Ravel et al. 2009; Fakhouri & Ma 2009; Darg et al. 2010; Lin et al. 2010; Kampczyk et al. 2012; Ellison et al. 2013). Major mergers can indeed trigger intense bursts of SF, thus shortening the overall SFH of galaxies (Mihos & Hernquist 1996; Gabor et al. 2010; Man & Belli 2018). In contrast, these red nuggets may have had a large reservoir of surrounding gas, which is gradually turned into stars over a much longer time-scale. If this scenario is true, then one should expect to find an anticorrelation between the H I column density and the DoR, which is however still too challenging to measure with the current radio telescopes.

6 SUMMARY AND CONCLUSIONS

In this seventh paper of the INSPIRE survey, we have investigated whether a correlation exists between the DoR and the local environment for the 52 UCMGs in the sample, as originally hinted at in FM17. We have started with cross-matching the INSPIRE catalogue with a catalogue of cluster candidates from the KiDS survey, obtained using the AMICO algorithm (Bellagamba et al. 2018, 2019; Maturi et al. 2019). Out of the 52 UCMGs, 45 are associated with a cluster as potential members, with a wide range of probabilities, SNR of the cluster detection, and cluster purity values.

We have estimated the local density and its significance with respect to the background around each galaxy in INSPIRE. To this aim, we have utilized ML based photometric redshift from the GAZNETS-1 catalogue (Li et al. 2022) and classification into quasars, galaxies, and stars from Feng et. al (submitted). This allowed us to identify galaxies with $m_r < 22$ situated within 1.5 Mpc of each INSPIRE UCMG, with a redshift difference of $\Delta z < 0.03$. We have then created a density map for each UCMG and estimated its significance over the background local density, obtained selecting 50 random region located around the UCMGs but at larger distances. We have finally assigned, on the basis of the analysis described above, two most likely environments (cluster or field) to each system in the INSPIRE sample.

These are the main results from the analysis presented in this paper:

(i) UCMGs can be found in all kind of environments, from dense clusters of galaxies to underdense field environments. Taking the classifications in Table 1 at face value, we have found 20 UCMGs in a cluster and 32 in the field. Of these systems, 9 are in a cluster and 18 are in the field with high-confidence environment classifications, while the remaining are only tentative.[5]

(ii) There is no clear correlation between the DoR and the probability for an UCMG to reside in a cluster for the entire sample. However, when restricting the analysis to the 'safe' detections (i.e. $P_{\rm cluster} \geq 0.5$) a linear relation emerges: the most extreme relics exhibit the highest $P_{\rm cluster}$ values, as illustrated in Fig. 2.

(iii) The density of the local environment where the UCMGs reside does not correlate with the DoR. However, UCMGs with an extended SFH (DoR < 0.3) tend to prefer less dense environments, as shown in Fig. 3. In fact, none of the objects with DoR ≤ 0.3 reside in a dense environment with high confidence. Only one could tentatively be in a group/cluster (J1154−0016).

(iv) A correlation is found between the DoR and the distance from the cluster centre $\log_{10} D$, for both techniques. Indeed, Fig. 8 illustrates that the higher the DoR, the closer the systems are to the centre of the overdensity. Additionally, the distances are comparable for the two methods ($2.6\,{\rm kpc} < \log_{10} D < 3.2$ kpc), at least for the high-confidence classifications.

In conclusion, our findings suggest that while a weak dependency on DoR exists, relics can be found across diverse environments with different local densities, consistent with both previous observational studies (FM17; Siudek et al. 2023) and hydrodynamical simulations (Peralta de Arriba et al. 2016; Flores-Freitas et al. 2022; Moura et al. 2024). However, younger UCMGs, with a DoR < 0.3 and thus characterized by a more extended SFH, are preferentially found in underdense environments and reside almost exclusively in the field. We argue that these results are justified by the premise that if a red nugget has formed in an overdensity at high redshift (or moved in quite early-on in cosmic time), the hot and dense ICM within the cluster gravitational potential has exerted high pressure and removed all the gas, hence quenching its SF activity (Peralta de Arriba et al. 2016; Boselli, Fossati & Sun 2022). In clusters, extreme relics did not interact with other members, because they possess very deep potential wells, also indicated by their large stellar velocity dispersion values, and incredibly high densities.

Conversely, in underdense environments, red nuggets at high-z that do not interact via mergers (growing in size) either keep forming stars at very low-rate consuming their gas envelope and becoming non-relics UCMGs, or they do not have any gas surrounding them

[5]Tortora et al. (2020) have found that the fraction of UCMGs in the field is slightly higher compared to that in clusters (see the right panel of their fig. 1). We confirm this result and remind the reader that the INSPIRE sample has been originally drawn from the same sample used in Tortora et al. (2020).

and hence evolve passively and undisturbed without companions to merge with, nor gas reservoir to form new stars.

Finally, we highlight that a fraction of the non-relics INSPIRE UCMGs in a cluster might also have been originated by stripping phenomena on an originally larger massive system, that have caused a compaction phase at later cosmic epochs (Dekel & Burkert 2014; van Dokkum et al. 2015).

Only by further extending the number of fully characterized and spectroscopically confirmed UCMGs, studying their stellar populations in great detail, we will be able to quantify the number densities of the different types of ultra-compact objects and study their evolution with redshifts. Current and upcoming surveys like *Euclid* (Euclid Collaboration: Mellier et al. 2024), *Vera C. Rubin* Observatory's Legacy Survey of Space and Time (*Rubin*–LSST; Ivezić et al. 2019, Multi-Object Spectroscopic Telescope (de Jong et al. 2019), and WHT Enhanced Area Velocity Explorer (WEAVE) at William Herschel Telescope (Jin et al. 2023) will be transformational in extending the number statistics and pushing the redshift boundaries between the near-by and the high-z Universe.

ACKNOWLEDGEMENTS

The research was carried out at the Jet Propulsion Laboratory, California Institute of Technology, under a contract with the National Aeronautics and Space Administration (80NM0018D0004), ©2024. All rights reserved. DS was supported by JPL, which is operated under a contract by Caltech for NASA. CS and CT acknowledge funding from the INAF PRIN-INAF 2020 program 1.05.01.85.11. GD acknowledges support by UKRI-STFC grants ST/T003081/1 and ST/X001857/1.

DATA AVAILABILITY

The INSPIRE data used in this paper are publicly available via the ESO Phase 3 Archive Science Portal under the collection INSPIRE (https://archive.eso.org/scienceportal/home?data_collection=INSPIRE, https:https://doi.eso.org/10.18727/archive/36).

REFERENCES

Bekki K., 2013, MNRAS, 438, 444
Bellagamba F. et al., 2019, MNRAS, 484, 1598
Bellagamba F., Roncarelli M., Maturi M., Moscardini L., 2018, MNRAS, 473, 5221
Benítez N., 2000, ApJ, 536, 571
Bialas D., Lisker T., Olczak C., Spurzem R., Kotulla R., 2015, A&A, 576, A103
Boselli A., Fossati M., Sun M., 2022, A&AR, 30
Boselli A., Gavazzi G., 2014, A&AR, 22
Byrd G., Valtonen M., 1990, ApJ, 350, 89
Cappellari M., 2013, ApJ, 778, L2
D'Ago G. et al., 2023, A&A, 672, A17, INSPIRE DR2
Daddi E. et al., 2005, ApJ, 626, 680
Damjanov I., Abraham R. G., McCarthy P. J., Glazebrook K., 2009, Apj, 695, 695
Damjanov I., Geller M. J., Zahid H. J., Hwang H. S., 2015a, ApJ, 806, 158
Damjanov I., Zahid H. J., Geller M. J., Hwang H. S., 2015b, ApJ, 815, 104
Darg D. W. et al., 2010, MNRAS, 401, 1552
de Jong J. T. A. et al., 2017, A&A, 604, A134
de Jong R. S. et al., 2019, The Messenger, 175, 3
de Ravel L. et al., 2009, A&A, 498, 379
Dekel A., Burkert A., 2014, MNRAS, 438, 1870
DESI Collaboration, 2023, AJ, 168, 58
Ellison S. L., Mendel J. T., Patton D. R., Scudder J. M., 2013, MNRAS, 435, 3627
Epanechnikov V. A., 1969, Theor. Probab. Appl., 14, 153
Fakhouri O., Ma C.-P., 2009, MNRAS, 394, 1825
Feng Hai-Cheng et al., , R. Morpho-Photometric Classification of KiDS DR5 Sources Based on Neural Networks: A Comprehensive Star-Quasar-Galaxy Catalog, 2024, ApJS, P 18, https://arxiv.org/abs/2406.03797
Ferré-Mateu A., Trujillo I., Martín-Navarro I., Vazdekis A., Mezcua M., Balcells M., Domínguez L., 2017, MNRAS, 467, 1929 (FM17)
Ferré-Mateu A., Vazdekis A., Trujillo I., Sánchez-Blázquez P., Ricciardelli E., de la Rosa I. G., 2012, MNRAS, 423, 632
Flores-Freitas R., Chies-Santos A. L., Furlanetto C., De Rossi M. E., Ferreira L., Zenocratti L. J., Alamo-Martínez K. A., 2022, MNRAS, 512, 245
Foltz R. et al., 2018, ApJ, 866, 136
Furlong M. et al., 2015, MNRAS, 465, 722
Gabor J. M., Davé R., Finlator K., Oppenheimer B. D., 2010, MNRAS, 407, 749
Giocoli C. et al., 2021, A&A, 653, A19
Göller J., Joshi G. D., Rohr E., Zinger E., Pillepich A., 2023, MNRAS, 525, 3551
Grèbol-Tomàs P., Ferré-Mateu A., Domínguez-Sánchez H., 2023, MNRAS, 526, 4024
Hennig C. et al., 2017, MNRAS, 467, 4015
Hou L., Wang Y., 2016, A&A, 588, A39
Huertas-Company M., Shankar F., Mei S., Bernardi M., Aguerri J. A. L., Meert A., Vikram V., 2013, ApJ, 779, 29
Ingoglia L. et al., 2022, MNRAS, 511, 1484
Ivezić Ž. et al., 2019, ApJ, 873, 111
Jin S. et al., 2023, MNRAS, 530, 2688
Kampczyk P. et al., 2012, ApJ, 762, 43
Kapferer W., Sluka C., Schindler S., Ferrari C., Ziegler B., 2009, A&A, 499, 87
Kaviraj S., Tan K.-M., Ellis R. S., Silk J., 2011, MNRAS, 411, 2148
Khramtsov V. et al., 2019, A&A, 632, A56
Kimmig L. C., Remus R.-S., Seidel B., Valenzuela L. M., Dolag K., Burkert A., 2023, preprint (arXiv:2310.16085)
Kuijken K. et al., 2019, A&A, 625, A2
Kuijken K., 2011, The Messenger, 146, 8
Y., Mellier, et al., 2024, preprint (arXiv:2405.13491)
Lesci G. F. et al., 2022a, A&A, 659, A88
Lesci G. F. et al., 2022b, A&A, 665, A100
Levi M. E. et al., 2019, BAAS, 51, 57
Li R. et al., 2022, A&A, 666, A85
Lin L. et al., 2010, ApJ, 718, 1158
Ma C.-J., Ebeling H., Donovan D., Barrett E., 2008, ApJ, 684, 160
Maksymowicz-Maciata M. et al., 2024, MNRAS, 531, 2864, (MM24)
Man A., Belli S., 2018, Nat. Astron., 2, 695–697
Martín-Navarro I. et al., 2023, MNRAS, 521, 1408
Maturi M., Bellagamba F., Radovich M., Roncarelli M., Sereno M., Moscardini L., Bardelli S., Puddu E., 2019, MNRAS, 485, 498
Maturi M., Meneghetti M., Bartelmann M., Dolag K., Moscardini L., 2005, A&A, 442, 851
Merritt D., 1983, ApJ, 264, 24
Mihos J. C., Hernquist L., 1996, ApJ, 464, 641
Moura M. T., Chies-Santos A. L., Furlanetto C., Zhu L., Canossa-Gosteinski M. A., 2024, MNRAS, 528, 353
Naab T. et al., 2014, MNRAS, 444, 3357
Nipoti C., Treu T., Auger M. W., Bolton A. S., 2009, ApJ, 706, L86
Oser L., Ostriker J. P., Naab T., Johansson P. H., Burkert A., 2010, ApJ, 725, 2312
Peluso G. et al., 2022, ApJ, 927, 130
Peralta de Arriba L., Quilis V., Trujillo I., Cebrián M., Balcells M., 2016, MNRAS, 461, 156
Poggianti B. M., Moretti A., Calvi R., D'Onofrio M., Valentinuzzi T., Fritz J., Renzini A., 2013, ApJ, 777, 125
Puddu E. et al., 2021, A&A, 645, A9

Quilis V., Trujillo I., 2013, ApJ, 773, L8
Radovich M. et al., 2020, MNRAS, 498, 4303
Roediger E., Bruggen M., Owers M. S., Ebeling H., Sun M., 2014, MNRAS, 443, L114
Romanello M. et al., 2023, A&A, 682, A72
Scognamiglio D. et al., 2020, ApJ, 893, 4
Siudek M. et al., 2023, MNRAS, 523, 4294
Spiniello C. et al., 2021a, A&A, 646, A28, INSPIRE Pilot
Spiniello C. et al., 2021b, A&A, 654, A136, INSPIRE DR1
Spiniello C. et al., 2024, MNRAS, 527, 8793
Steinhauser D., Schindler S., Springel V., 2016, A&A, 591, A51
Stringer M., Trujillo I., Dalla Vecchia C., Martinez-Valpuesta I., 2015, MNRAS, 449, 2396
Tortora C. et al., 2016, MNRAS, 457, 2845
Tortora C. et al., 2018, MNRAS, 481, 4728
Tortora C. et al., 2020, A&A, 638, L11
Trujillo I., Cenarro A. J., de Lorenzo-Cáceres A., Vazdekis A., de la Rosa I. G., Cava A., 2009, ApJ, 692, L118
Trujillo I., Conselice C. J., Bundy K., Cooper M. C., Eisenhardt P., Ellis R. S., 2007, MNRAS, 382, 109
Trujillo I., Ferré-Mateu A., Balcells M., Vazdekis A., Sánchez-Blázquez P., 2014, ApJ, 780, L20
van Dokkum P. G. et al., 2010, ApJ, 709, 1018
van Dokkum P. G. et al., 2015, ApJ, 813, 23
van Dokkum P. G., 2008, ApJ, 674, 29
Wellons S. et al., 2016, MNRAS, 456, 1030
Wright A. H. et al., 2019, A&A, 632, A34

This paper has been typeset from a TEX/LATEX file prepared by the author.